Supporting Information

van Loo et al. 10.1073/pnas.0903951107

SI Text

Materials and Methods. ***Materials.*** Phosphate **1a**, phosphonate **4b**, and sulfate **5b** (Fig. 1) were obtained from Sigma, phosphates **1b** and **2a** from Aldrich. Phosphate **3b** was obtained from Riedel de Haen. Phosphate **2b**, phosphonate **4a**, sulfate **5a**, and sulfonates **6a** and **6b** were synthesized as described below. Streptactin protein resin and the pASKIBA5plus plasmid DNA were obtained from Stratech Scientific. All DNA modifying enzymes were from New England Biolabs except for *Pfu* DNA polymerase (Stratagene). Oligonucleotides were supplied by SigmaGenosys. All constructs were sequenced at the sequencing facility of the Department of Biochemistry, University of Cambridge.

Preparation of substrates. Commercially available phosphates **1a**, **1b**, **2a**, and **3b** and phosphonate **4b** (Fig. 1) were used as supplied by the manufacturer.

p-nitrophenyl ethylphosphate (**2b**) was synthesized as described previously (1). ^{1}H NMR and ESI-MS analysis confirmed that the correct product was obtained.

Phenyl phenylphosphonate (**4a**) was synthesized by dropwise addition of a solution of phenol (0.94 g, 0.01 mol) and pyridine (0.97 mL, 0.012 mol) in diethyl ether over 1 h to a solution of phenylphosphonic dichloride (2.13 mL, 0.015 mol) in diethyl ether at room temperature under argon and left stirring for 12 h. The resulting white precipitate was filtered and washed with water and 10% HCl. The ether layer was dried with Na_2SO_4 and the solvent removed under reduced pressure. The resulting brown oil was separated on silica gel eluting with dichloromethane/methanol (50∶1). The resulting white solid was the target product **4a** (1.05 g, 0.004 mol, 45% yield): $C_{12}H_{11}O_3P$ M_r 234.19, ^{1}H NMR ($CDCl_3$) δ 6.89 (s, 1H), 7.06–7.09 (m, 3H), 7.19–7.21 (m, 2H), 7.40–7.44 (m, 2H), 7.52–7.56 (m, 1H), 7.78–7.83 (m, 2H); ^{1}H NMR (d_6-DMSO) δ 7.07–7.10 (m, 3H), 7.25–7.29 (m, 2H), 7.40–7.57 (m, 3H), 7.72–7.76 (m, 2H); ESI M-H$^-$ 233.1, MH$^+$ 235.2.

Phenyl sulfate (**5a**) was synthesized by adding chlorosulfonic acid (1.33 mL, 0.02 mol) dropwise to phenol (1.88 g, 0.02 mol) dissolved in a mixture of dry dichloromethane and dry pyridine at −15 °C. The reaction was allowed to come to room temperature and was stirred overnight. Then 20 mL of 0.5 g mL^1 K_2CO_3 was added. The obtained white solid was washed with diethyl ether and subsequently dissolved in H_2O. The aqueous solution was adjusted to pH 5 with acetic acid and extracted with diethyl ether to remove any remaining phenol. H_2O was evaporated under reduced pressure, and the white solid was recrystallized from hot ethanol/H_2O. The obtained crystals were dried under high vacuum. A comparison of the UV-visible (UV-vis) spectra of a solution of this solid prior to and after complete hydrolysis of the resulting mixture by *Pseudomonas aeruginosa* aryl sulfatase (2) showed that the mixture contained ∼60% of the sulfate **5a**. ^{1}H NMR (D_2O) δ 7.21–7.42 (m, 3H), 7.35–7.44 (m, 2H), ESI, M$^+$ 173.11 (acid form).

p-nitrophenyl sulfate (**5b**). UV-vis spectra suggested that the commercial preparation of sulfate **5b** was contaminated with *p*-nitrophenol. To remove this contamination the commercial preparation was dissolved in 44 mM succinic acid, 33 mM imidazole, 33 mM diethanolamine (SID), and the resulting solution was adjusted to pH 5.0 with acetic acid. The solution was washed with diethyl ether to selectively extract *p*-nitrophenol. The organic phase was back extracted with 0.1 M NaOH. After two washes the reverse extraction into 0.1 M NaOH was no longer yellow indicating that all *p*-nitrophenol had been removed from the sulfate monoester containing solution. The remaining diethyl ether was removed in vacuo. The concentration of sulfate **5b** was determined by adding *P. aeruginosa* aryl sulfatase (2) to a dilute solution of substrate and incubated for several hours at pH 8.0 and subsequent determination of the concentration of released *p*-nitrophenol by absorbance measurements at 400 nm.

Phenyl phenylsulfonate (**6a**) was synthesized by dropwise addition of benzenesulfonyl chloride (1.3 mL, 0.01 mol) to a solution of phenol (0.94 g, 0.01 mol) and triethylamine (1.7 mL, 0.012 mol) in THF at 0 °C under argon. The solution was allowed to come to room temperature and left stirring for 12 h, after which a white precipitate resulted. The solution was filtered, diethyl ether was added, and the solution was washed with saturated $NaHCO_3$ solution and water. The organic solvent layer was dried with Na_2SO_4 and the solvent removed under reduced pressure; a brown oil resulted. The oil was separated on silica gel eluting with cyclohexane/ethylacetate (50∶1), and a clear colorless oil resulted (0.87 g, 0.004 mol, 37% yield): $C_{12}H_{10}O_3S$ M_r 234.27, ^{1}H NMR ($CDCl_3$) δ 6.95–6.97 (m, 2H), 7.23–7.29 (m, 3H), 7.49–7.52 (m, 2H), 7.63–7.66 (m, 1H), 7.81–7.83 (m, 2H); ESI M-H$^-$ 233.3, MH$^+$ 235.4.

p-nitrophenyl phenylsulfonate (**6b**) was synthesized by adding benzenesulfonylchloride (2.6 mL, 0.02 mol) dropwise to *p*-nitrophenol (2.48 g, 0.02 mol) dissolved in dry pyridine at 0 °C. The reaction was allowed to come to room temperature and was stirred overnight. Pyridine was evaporated under reduced pressure, and the remaining solids were dissolved in chloroform. The organic phase was washed with saturated $NaHCO_3$ solution (2×) and water (1×) and subsequently dried by using anhydrous Na_2SO_4. Chloroform was removed under reduced pressure. The resulting crystalline material was washed with EtOAc:hexane 1:9, resulting in light brown crystals (4.10 g, 0.015 mol 75% yield). ^{1}H NMR ($CDCl_3$) δ 7.12–7.19 (m, 2H), 7.50–7.58 (m, 2H), 7.65–7.74 (m, 1H), 7.80–7.88 (m, 2H), 8.12–8.19 (m, 2H); ESI M$^+$ 279.3.

Cloning of BcPMH and mutant construction. The gene encoding PMH from *Burkholderia caryophilli* PG2952 (*Bc*PMH) (accession number U44852) (3) was amplified by PCR from plasmid pMON9428 (Monsanto) and cloned into the N*co*I/P*st*I restriction sites of pBAD*myc*HisA for the untagged protein and into *Xho*I/*Pst*I sites of pASK-IBA5plus for the N-terminally Strep-tagged protein. Cloning of the *Bc*PMH gene into the *Nco*I site of the pBAD*myc*HisA vector required the introduction of an extra alanine codon directly after the start codon. Expression of the gene in the pASK-IBA5plus vector results in a translational fusion with an N-terminal Strep-tag (Trp-Ser-His-Pro-Gln-Phe-Glu-Lys). Primers [forward pBAD*myc*HisA: 5′CGC GCG GCC ATG GCA ACC AGA AAA AAT GTC CTG CTT ATC GTC3′; forward pASK-IBA5plus 5′GCG CGC CTC GAG CAT GAC CAG AAA AAA TGT CCT GCT TAT C3′′ reverse (both constructs): 5′CGC GCG CTG CAG TCA ATG GTT GCG CGT TGT CAG CCC3′] were used at 0.4 nM in a reaction with 0.2 mM dNTPs and 0.05 U μL^{-1} *Pfu*Turbo DNA polymerase. The temperature program used was 15 min at 95 ºC without polymerase, followed by 30 cycles of 60 s 95 ºC, 45 s 68 ¨C − 0.5 ¨C cycle^{-1} (each cycle the temperature of this segment was lowered by 0.5 ºC), 180 s 72 ºC, and finished with 4 min at 72 ºC. The PCR products for the untagged and tagged constructs were digested with *Nco*I*Pst*I and *Xho*I*Pst*I, respectively, and subsequently ligated into *Nco*I*Pst*I digested pBAD*myc*HisA or *Xho*I*Pst*I digested pASK-IBA5plus plasmid DNA using T4 DNA ligase. The ligation mixture was transformed into *E. coli* TOP10 by using

electroporation. The transformants were plated on LB medium containing ampicillin (100 mg L^{-1}). Colonies were checked for the presence of the insert by using a PCR with *Taq* polymerase and colony material as the template. Positive colonies were used to inoculate 5 mL of liquid LB medium and grown overnight at 37 ºC. Plasmid DNA was extracted and the insert was sequenced. The active site cysteine (Cys57) was replaced by alanine by using the QuikChange method (Stratagene) with pASK-IBA5plus *Bc*PMH as the template.

Protein expression and purification. Protein from the various plasmids was expressed in *E. coli* BL21(DE3) in TY (16 g/L bacto tryptone; 10 g/L yeast extract; 10 g/L NaCl) or TB [12 g/L bacto tryptone; 24 g/L yeast extract; 4% (vol/vol) glycerol; 0.1 M potassium phosphate] medium containing 100 mg/L ampicillin and 50 mg/L kanamycin at 28 °C. Apart from the protein used for crystallization, both the tagged and untagged proteins were coexpressed with *Mtb*FGE (4, 5) to ensure a higher degree of fGly modification. For testing the presence of contaminants originating from *E. coli*, cells containing pASKIBA5plus and pSJMF1 were treated the same way as those expressing the tagged protein.

Untagged *Bc*PMH was purified by using anion exchange (Q-Sepharose), hydrophobic interaction (Phenyl Sepharose), and size exclusion (Superdex 200) chromatography. Strep-tagged *Bc*PMH was purified by using Strep-tactin affinity purification followed by a size exclusion step.

Expression of *Mtb*FGE from the pSJMF1 construct (5) was induced by adding 1 mM IPTG to a cell culture at $OD_{600} \sim 0.2$ approximately 15–30 minutes prior to induction of the expression of the *Bc*MPH gene. Expression from the pBAD*myc*HisA*Bc*PMH construct was induced by addition of 0.02% (wt/vol) L-arabinose followed by overnight growth. Expression of the tagged enzyme from the pASKIBA5plus*Bc*PMH constructs was induced by adding 200 μg/L anhydrotetracyclin.

Cells expressing the untagged *Bc*PMH were harvested by centrifugation and resuspended in 20 mM Bistris propane pH 9.0. One tablet of Complete EDTA-Free protease inhibitor cocktail per 12 g of wet cell pellet weight was added to the suspension, and the cells were lysed in an emulsiflex-C5 homogenizer (Avestin). Cell-free extract (CFE) was obtained by centrifugation of the cell lysate at $30,000 \times g$ for 90 min. The subsequent anion exchange and hydrophobic interaction chromatography were essentially done as described before (3). Active fractions that eluted from the hydrophobic interaction column were pooled and concentrated to a protein concentration of around 15 mg/mL and subsequently loaded on a Superdex 200 size exclusion column that was running in 100 mM Bistris propane pH 7.5–9.0, 150 mM KCl. The protein eluted at the expected molecular weight corresponding to a tetrameric enzyme (3). The protein containing fractions were pooled, concentrated, and desalted into 10 mM Bistris propane pH 9.0. Small aliquots of the protein were flash-frozen in liquid nitrogen and subsequently stored at 20 °C. Typical yields were around 2 mg pure protein per gram of wet cells.

For purification of the Strep-tagged enzyme a CFE was made as described for the untagged enzyme, except that the cells were resuspended in 20 mL of 100 mM Tris-HCl pH 8.0, 150 mM NaCl. The enzyme was purified from CFE by loading an appropriate volume of CFE (1–3 mL depending on protein content) onto a 1-mL gravity-flow column of Strep-tactin resin. After loading the nonbinding proteins were washed off with 100 mM Tris-HCl pH 8.0, 150 mM NaCl. The tagged enzyme was eluted with 2.5 mM d-desthiobiotin in 100 mM Tris-HCl pH 8.0, 150 mM NaCl. The column material was regenerated according to the manufacturer's instructions. This procedure could be repeated several times depending on the requirement for protein. Active fractions were pooled, concentrated, and subsequently loaded onto a Superdex 200 column that was running under the same conditions as for the untagged protein. Active fractions were pooled, concentrated, desalted, and stored as described for the untagged variant. Typical yields were around 6–7 mg pure protein per gram of wet cells.

Anaerobic protein expression and purification. To obtain Strep-*Bc*PMH without fGly conversion, protein expression and affinity purification were performed under anaerobic conditions. A culture of the *E. coli* strain expressing the protein *Bc*PMH grown under aerobic conditions was used to inoculate 100 mL of LB medium supplemented with ampicillin (100 mg L^{-1}). Bacteria were grown overnight under anaerobic conditions in a glove box (Bactron IV) with a nitrogen/hydrogen/carbon dioxide (85/5/10) atmosphere. Another 100-mL LB medium supplemented with ampicillin were inoculated with this culture and grown anaerobically. This culture was then used to inoculate three flasks of 1 L of LB medium supplemented with ampicillin and grown to an OD_{600} of 0.25. Strep-*Bc*PMH was expressed as described above but under the nitrogen/hydrogen/carbon dioxide atmosphere. The cells were transferred anaerobically into centrifuge tubes, then harvested by centrifugation at $4,000 \times g$ for 20 min at 4 °C, outside the glove box, and resuspended under anaerobic conditions in degassed washing buffer (100 mM Tris-HCl pH 8.0, 150 mM NaCl). Strep-*Bc*PMH was from whole cells purified as described above, performing all steps under anaerobic conditions, with the exception of the centrifugation of the crude lysate and the size exclusion chromatography. All buffers were degassed prior to use.

Determination of background rates. The rates for the uncatalyzed reactions for substrates **1a**–**2b** and **5a,b** could be derived from published literature data (details in the footnotes to Table S1).

Hydrolysis of phosphate triester **3b** in 20 mM Bistris propane (at pH 7.5, 100 mM KCl) was monitored at 400 nm. The resulting V_{obs} (in M s^{-1}) was plotted against the substrate concentration. These results could be fitted to the equation $V_{obs} = k_{uncat}{}^{*}$ [phosphate triester **3b**], and the resulting data are displayed in Table S1.

Conversion of phosphonate monoester **4b** was too slow to be detected at 30 °C at pH 7.5. The dependency of hydrolysis on the concentration of hydroxide (k_{OH} in M^{-1} s^{-1}) at 30 °C was fast enough to be determined by fitting initial rates. At a fixed substrate concentration, initial rates (k_{obs} in s^{-1}) were determined at varying concentrations of KOH. The data could be fitted to $k_{obs} = k_{OH}{}^{*}$ [OH^-]. The resulting k_{OH} was used to calculate k_{uncat} at pH 7.5 by using the same formula in which pH 7.5 corresponds to a [OH^-] of $10^{-(14-7.5)} = 3.2 \times 10^{-7}$ M. Hydrolysis rates of phosphonate **4a** were calculated from the k_{uncat} for phosphonate monoester **4b** by using a Brønsted value of −0.69 for the chemical hydrolysis of aryl methylphosphonates (6) and pK values for *p*-nitrophenol and phenol of 7.14 and 9.98, respectively.

Background rates for sulfonate monoesters **6a** and **6b** were derived as described above for phosphonate **4b** from experimentally determined k_{OH} values. k_{OH} **6a** $= 4.4 * 10^{-4}$ s^{-1}; k_{OH} **6b** $= 1.7 * 10^{-2}$ s^{-1}. Both k_{OH} values were determined by measuring from initial rates of product formation (phenolate or 4-nitrophenolate), monitored by an increase of absorbance at a fixed wavelength, at increasing OH^- concentrations.

Product analysis. Several techniques were used to support the proposed mechanism of product formation.

Enzymatic reaction in the presence of ^{18}O-labeled H_2O. Substrates **1b**–**6b** were incubated in 9.5% (vol/vol) $H_2{}^{18}O$ in SID of 1,3-bis[tris(hydroxymethyl)methylamino]propane buffer pH 7.5 or 8.0 in the presence of an appropriate concentration enzyme for 0.5–72 h and subsequently analyzed by using liquid chromatography mass spectrometry (Department of Chemistry, University of Cambridge). The ES^- trace of the *p*-nitrophenol is shown in Fig. S2*C*.

Product identification.
(a) Thin layer chromatography (TLC). To confirm the identity of the product (i.e., emergence of the 4-nitrophenyl leaving group), ~0.2–5 mM of substrates **1b–6b** was allowed to react in the presence of phosphonate monoester hydrolase (PMH) (1–20 μM, 12–24 h in 50 mM Tris-HCl, pH 8.0), and a yellow product emerged, whose spectrum was identical to 4-nitrophenolate (see below). When the product mixture was acidified to pH ~ 2, the yellow color disappeared, consistent with the presence of *p*-nitrophenol. The acidified solutions were extracted with diethyl ether. The diethyl ether extracts were analyzed by TLC (SiO_2, EtOAc: 96% EtOH, 19:1) and showed a yellow spot. The R_f values (0.38) of these spots were identical to authentic *p*-nitrophenol. When the reference compound was spotted on top of the substrate incubations, only one single yellow spot was observed at the expected R_f value, providing further evidence that the product and 4-nitrophenol are identical. No additional products can be detected with UV light (254 nm).

(b) HPLC. The above-mentioned incubations of substrate and enzyme were also analyzed by reverse phase HPLC (on an ACE 5 C18-300 column, 4.6 × 250 mm, flow 1.0 mL min^{-1}; gradient 10–100% acetonitrile in 0.1% (vol/vol) trifluoroacetic acid in H_2O). All incubations showed *p*-nitrophenol eluting at the same retention time as an authentic sample of *p*-nitrophenol (eluting around 40% acetonitrile).

(c) UV-vis. The above-mentioned incubations of substrate and enzyme were also analyzed by UV-vis spectroscopy. The spectrum from 370 to 500 nm was identical in shape to authentic *p*-nitrophenol for each conversion.

(d) ^{31}P-NMR. Compounds **1b**, **2b**, and **4b** (~10 mg in 700–800 μL 50 mM Tris-HCl pH 8.0 were incubated in the presence and absence of PMH (2–100 μM) for 12–24 h, after which up to ~20% (vol/vol) D_2O was added. The samples were then analyzed by ^{31}P-NMR (400 MHz, Bruker DPX400). Chemical shifts for the substrates and products were in the expected ranges (7): inorganic phosphate: 2.3–3.1 ppm (8); phosphate monoester **1b**: 0.18–0.22 ppm (9); phosphate diester **2b**: −4.2 to −4.9 ppm; ethylphosphate: 3.4 ppm; phosphonate monoester **4b**; 13.6 ppm; phenylphosphonate: 12.1–13.0 ppm. Spiking with authentic product samples was used to further ascertain product identity. In each case the peak identified as corresponding to product was increased by the addition of an authentic sample of presumed product and no additional peaks arose.

In the case of phosphate triester **3b**, only approximately 0.1 mg of product was produced in 24 h (in the presence of 100 μM PMH in 1 ml total volume), making detection of the phosphate-containing product by ^{31}P-NMR difficult. However, 4-nitrophenyl product was detected for this reaction by TLC [see (*a*)] in addition to UV-active baseline material (consistent with the final monoester product).

Enzyme assays. All enzyme assays were performed in 44 mM succinic acid, 33 mM imidazole, 33 mM diethanolamine (SID) or in the case of phosphate triester **3b** in 20 mM Bistris propane, 100 mM KCl because of high background hydrolysis of phosphate triester **3b** in SID. Enzymatic hydrolysis of compounds **1b–6b** was followed by monitoring the release of *p*-nitrophenol at 400 nm by using a SpectraMax Plus multiwell reader for substrates **1b**, **2b**, and **4b–6b**. Hydrolysis of phosphate triester **3b** was monitored in a Cary 100 Bio UV-vis spectrophotometer (Varian) in a 1-cm glass cuvette. Initial rate measurements were carried out in duplicate and the data averaged prior to fitting to Eq. S1 or S2 as described below. The extinction coefficients of *p*-nitrophenol at varying pH for both the multiwell reader and the Cary 100 were determined for pH 6.0–10.0. The errors represented in Tables 1–3 are the statistical errors from each fit.

Enzymatic hydrolysis of substrates **1a**, **2a**, and **4a–6a** was monitored at 270–280 nm, depending on the optimal difference in absorption between the product and the substrate. Hydrolysis of compounds **2a** and **4a** was sufficiently fast to use initial rate measurements. The K_M values for compounds **1a**, **5a**, and **6a** were determined by using the competitive inhibition constants for the conversion of phosphate diester **2b** (Fig. S4). The k_{cat} values for these three compounds were then obtained from a single spectrophotometric trace as described below (Eqs. S3 and S4).

Fitting of enzyme kinetics.

Kinetic parameters via initial rates.
To determine the kinetic parameters for substrates with *p*-nitrophenol as the leaving group as well as for substrates **2a** and **4a**, the initial rates in μmol min^{-1} mg^{-1} (V_{obs}) at varying substrate concentrations were fitted to the various models described.

Normal Michaelis–Menten kinetics (substrates **1b**, **3b**, **5b**, and **6b**)

$$V_{obs} = \frac{V_{max} \times [S]}{K_M + [S]}. \qquad \textbf{[S1]}$$

Substrate inhibition kinetics (substrates **2a,b** and **4a,b**)

$$V_{obs} = \frac{V_{max}{}^{app} \times [S]}{K_M{}^{app} + [S] + \frac{[S]^2}{K_{si}}}. \qquad \textbf{[S2]}$$

Kinetic parameters from a single spectrophotometric trace.
The K_M values for substrates **1a**, **5a**, and **6a** were assumed to be equal to the competitive inhibition constant (K_{ic}) of the respective compounds on the enzymatic conversion of phosphate diester **2b** (see below for more details). These K_M values were subsequently used as a constant in least squares numerical fitting of a single spectrophotometric trace of the conversion of these substrates recorded at various wavelengths to Eqs. S3 and S4 by using Micromath Scientist, similar to a procedure previously used to determine enzyme kinetics from progress curves of epoxide hydrolases (10–12).

$$A = \varepsilon_{substrate} \times d \times [S] - \varepsilon_{product(s)} \times d \times ([S]_0 - [S]), \qquad t = 0,$$
$$[S] = [S]_0 - [P]_0, \qquad \textbf{[S3]}$$

$$\frac{d[S]}{dt} = -\frac{k_{cat} \times [Enz] \times [S]}{K_M + [S]}, \qquad \textbf{[S4]}$$

in which A is the absorbance at appropriate wavelength, [S] is the substrate concentration during the reaction (mM), $[S]_0$ is the substrate concentration added of the reaction (mM), $[P]_0$ is the product formed at $T = 0$ as a result of the time lost between addition of the enzyme and the placement of the cuvette into the spectrophotometer (mM), [Enz] is the enzyme concentration (mM), d is the path length of the cuvette in centimeters, and $\varepsilon_{substrate}$ and $\varepsilon_{product(s)}$ are the extinction coefficients of the substrate and product(s), respectively (mM^{-1} cm^{-1}).

Cross-inhibition experiments.
Inhibition of the conversion of phosphate diester **2b** by promiscuous substrates **1a**, **1b**, **3b**, **5a**, **5b**, **6a**, and **6b** was monitored by recording Michaelis–Menten plots of phosphate diester **2b** conversion in the presence of increasing concentrations of each promiscuous substrate. Each of these curves was fitted to Eq. S1, because the conditions were chosen in such a way that the effect of substrate inhibition was negligible. The resulting apparent values of k_{cat} and K_M were used to calculate $k_{cat}{}^{app}/K_M{}^{app}$, which were plotted against the inhibitor concentration ([I]) and fitted to

Eq. S5. The resulting K_{ic} values were either compared with the K_M values of the inhibitors or used as constants in the kinetic measurement as described above.

$$\frac{k_{cat}{}^{app}}{K_M{}^{app}} = \frac{k_{cat}/K_M}{1 + \frac{[I]}{K_{ic}}}. \quad [S5]$$

pH-rate profile fitting.
Values for each parameter k_{cat} and k_{cat}/K_M for substrates **1b**, **2b**, **3b**, **4b**, **5b**, and **6b** were determined at pH values in the range of pH 6.0–10 with 0.5 pH-scale increments. The pH dependencies of k_{cat} and k_{cat}/K_M were fitted to the various models described below, in which K represents the respective kinetic parameter and K_{ind} is the proportion of the value of that parameter that is independent of pH for pH 6.0–10.0.

I. Model in which the process represented by $K_{lim}1$ is linked to the protonated state of one ionizable group.
Model I:

$$K = K_{ind} + \frac{K_{lim}}{\left(1 + \frac{K_a}{[H^+]}\right)}. \quad [S6]$$

II. Model in which the process represented by $K_{lim}1$ is linked to the protonated state of one group and the deprotonated state of another.
Model II:

$$K = K_{ind} + \frac{K_{lim}1}{\left(1 + \frac{[H^+]}{K_a1}\right) \times \left(1 + \frac{K_a2}{[H^+]}\right)}. \quad [S7]$$

MALDI-TOF. MALDI-TOF mass spectrometry analyses were performed by L. Packman (PNAC Facility, University of Cambridge). MALDI-TOF of a tryptic digest of *Bc*PMH was used to demonstrate the presence of a formylglycine modification as described (5). To compare the degree of fGly modification in anaerobically expressed and *Mtb*FGE-coexpressed *Bc*PMH, samples of both protein preparations were subjected to trypsin digestion at pH 8 for 16 h. After reduction by 5 mM tris(2-carboxyethyl)phosphine from neutralized stock for 30 min at room temperature, the samples were alkylated with 34 mM acrylamide for 1.75 h at room temperature. Completeness of alkylation was checked on two cysteine-containing peptides, and samples were directly subjected to MALDI-TOF analysis in an α-cyano-4-hydroxycinnamic acid matrix. Only the Cys57-containing peptide (49-NHVTTCVPCGPAR-61) was detected reliably above background. The ionization efficiency of the fGly57-containing peptide in the CHCA matrix was not high enough to provide a signal above background for both enzyme preparations.

microPIXE. The microPIXE experiment (13) was carried out at the University of Surrey Ion Beam Centre as described before (5). Sulfur atoms served as the internal quantitative standard to calculate metal ion occupancy.

Crystallization, data collection, structure determination, and analysis. Crystals were grown at 18 °C by the hanging drop vapor diffusion method with equal volumes of protein (10 mg/mL) and reservoir buffer (2 μL total). Strep-*Bc*PMH crystals started appearing after two weeks in a solution containing 0.1 M MES pH 6.5, 20% (wt/vol) PEG 5000 monomethyl ether, 0.3 M $(NH_4)_2SO_4$. Before flash freezing in liquid nitrogen, the crystals were soaked in the crystallization buffer supplemented with 15% (vol/vol) glycerol for cryoprotection.

Diffraction of Strep-*Bc*PMH crystals extended to 2.4 Å at the X-ray Diffraction Data Collection Facilities, Department of Biochemistry, University of Cambridge (rotating copper anode). The dataset was collected at a wavelength of 1.5418 Å on an Raxis IV image plate and processed by using the XDS package (14). Statistics are displayed in Table S3. The structure of Strep-*Bc*PMH was solved by molecular replacement using Amore with *Rl*PMH (Protein Data Bank ID: 2vqr) as a search model (15). Iterative cycles of model building and refinement were carried out with COOT and REFMAC5 (16, 17).

1. Hendry P, Sargeson AM (1989) Metal ion promoted phosphate ester hydrolysis. Intramolecular attack of coordinated hydroxide ion. *J Am Chem Soc* 111:2521–2527.
2. Beil S, et al. (1995) Purification and characterization of the arylsulfatase synthesized by *Pseudomonas aeruginosa* PAO during growth in sulfate-free medium and cloning of the arylsulfatase gene (*atsA*). *Eur J Biochem* 229:385–394.
3. Dotson SB, Smith CE, Ling CS, Barry GF, Kishore GM (1996) Identification, characterization, and cloning of a phosphonate monoester hydrolase from *Burkholderia caryophilli* PG2982. *J Biol Chem* 271:25754–25761.
4. Carrico IS, Carlson BL, Bertozzi CR (2007) Introducing genetically encoded aldehydes into proteins. *Nat Chem Biol* 3:321–322.
5. Jonas S, van Loo B, Hyvonen M, Hollfelder F (2008) A new member of the alkaline phosphatase superfamily with a formylglycine nucleophile: Structural and kinetic characterisation of a phosphonate monoester hydrolase/phosphodiesterase from *Rhizobium leguminosarum*. *J Mol Biol* 384:120–136.
6. McWhirter C, et al. (2008) Mechanistic study of protein phosphatase-1 (PP1), a catalytically promiscuous enzyme. *J Am Chem Soc* 130:13673–13682.
7. Cade-Menun BJ (2005) Characterizing phosphorus in environmental and agricultural samples by ^{31}P nuclear magnetic resonance spectroscopy. *Talanta* 66:359–371.
8. Gorenstein DG (1984) *Phosphorus-31 NMR: Principles and Applications* (Academic, London), p. 604.
9. Domingos JB, Longhinotti E, Bunton CA, Nome F (2003) Reactions of bis(2,4-dinitrophenyl) phosphate with hydroxylamine. *J Org Chem* 68:7051–7058.
10. Rink R, et al. (1999) Mutation of tyrosine residues involved in the alkylation half reaction of epoxide hydrolase from *Agrobacterium radiobacter* AD1 results in improved enantioselectivity. *J Am Chem Soc* 121:7417–7418.
11. van Loo B, Kingma J, Arand M, Wubbolts MG, Janssen DB (2006) Diversity and biocatalytic potential of epoxide hydrolases identified by genome analysis. *Appl Environ Microbiol* 72:2905–2917.
12. van Loo B, et al. (2004) Directed evolution of epoxide hydrolase from *A. radiobacter* toward higher enantioselectivity by error-prone PCR and DNA shuffling. *Chem Biol* 11:981–990.
13. Garman EF, Grime GW (2005) Elemental analysis of proteins by microPIXE. *Prog Biophys Mol Biol* 89:173–205.
14. Kabsch W (1993) Automatic processing of rotation diffraction data from crystals of initially unknown symmetry and cell constants. *J Appl Cryst* 26:795–800.
15. Navaza J (1994) AMoRe: An automated package for molecular replacement. *Acta Crystallogr A* 50:157–163.
16. Emsley P, Cowtan K (2004) Coot: Model-building tools for molecular graphics. *Acta Crystallogr D* 60:2126–2132.
17. Murshudov GN, Vagin AA, Dodson EJ (1997) Refinement of macromolecular structures by the maximum-likelihood method. *Acta Crystallogr D* 53:240–255.
18. Benjdia A, Deho G, Rabot S, Berteau O (2007) First evidences for a third sulfatase maturation system in prokaryotes from *E. coli aslB* and *ydeM* deletion mutants. *FEBS Lett* 581:1009–1014.
19. Benkovic SJ, Benkovic PA (1966) Studies on sulfate esters. I. Nucleophile reactions of amines with *p*-nitrophenyl sulfate. *J Am Chem Soc* 88:5504–5511.
20. Kirby AJ, Jencks WP (1965) The reactivity of nucleophilic reagents toward the *p*-nitrophenyl phosphate dianion. *J Am Chem Soc* 87:3209–3216.
21. Kirby AJ, Vargolis AG (1967) The reactivity of phosphate esters. Monoester hydrolysis. *J Am Chem Soc* 89:415–423.
22. Zalatan JG, Herschlag D (2006) Alkaline phosphatase mono- and diesterase reactions: Comparative transition state analysis. *J Am Chem Soc* 128:1293–1303.
23. Khan SA, Kirby AJ (1970) The reactivity of phosphate esters. Multiple structure-activity correlations for the reactions of triesters with nucelophiles. *J Chem Soc B* 1172–1182.
24. McWhirter C, et al. (2008) Mechanistic study of protein phosphatase-1 (PP1), a catalytically promiscuous enzyme. *J Am Chem Soc* 130:13673–13682.
25. D'Rozario P, Smyth RL, Williams A (1984) Evidence for a single transition state in the intermolecular transfer of a sulfonyl group between oxyanion donor and acceptors. *J Am Chem Soc* 106:5027–5028.
26. Kirby AJ, Vargolis AG (1967) The reactivity of phosphate esters. Monoester hydrolysis. *J Am Chem Soc* 89:415–423.
27. Kirby AJ, Jencks WP (1965) The reactivity of nucleophilic reagents toward the *p*-nitrophenyl phosphate dianion. *J Am Chem Soc* 87:3209–3216.
28. Chin J, Banaszczyk M, Jubian V, Zou X (1989) Co(III) complex promoted hydrolysis of phosphate diesters: Comparison in reactivity of rigid *cis*-diaquotetraazacobalt(III) complexes. *J Am Chem Soc* 111:186–190.
29. Purcell J, Hengge AC (2005) The thermodynamics of phosphate versus phosphorothioate ester hydrolysis. *J Org Chem* 70:8437–8442.
30. Nikolic-Hughes I, Rees DC, Herschlag D (2004) Do electrostatic interactions with positively charged active site groups tighten the transition state for enzymatic phosphoryl transfer? *J Am Chem Soc* 126:11814–11819.
31. Nikolic-Hughes I, O'Brien PJ, Herschlag D (2005) Alkaline phosphatase catalysis is ultrasensitive to charge sequestered between the active site zinc ions. *J Am Chem Soc* 127:9314–9315.
32. Fendler EJ, Fendler JH (1968) Hydrolysis of nitrophenyl and dinitrophenyl sulfate esters. *J Org Chem* 33:3852–3859.

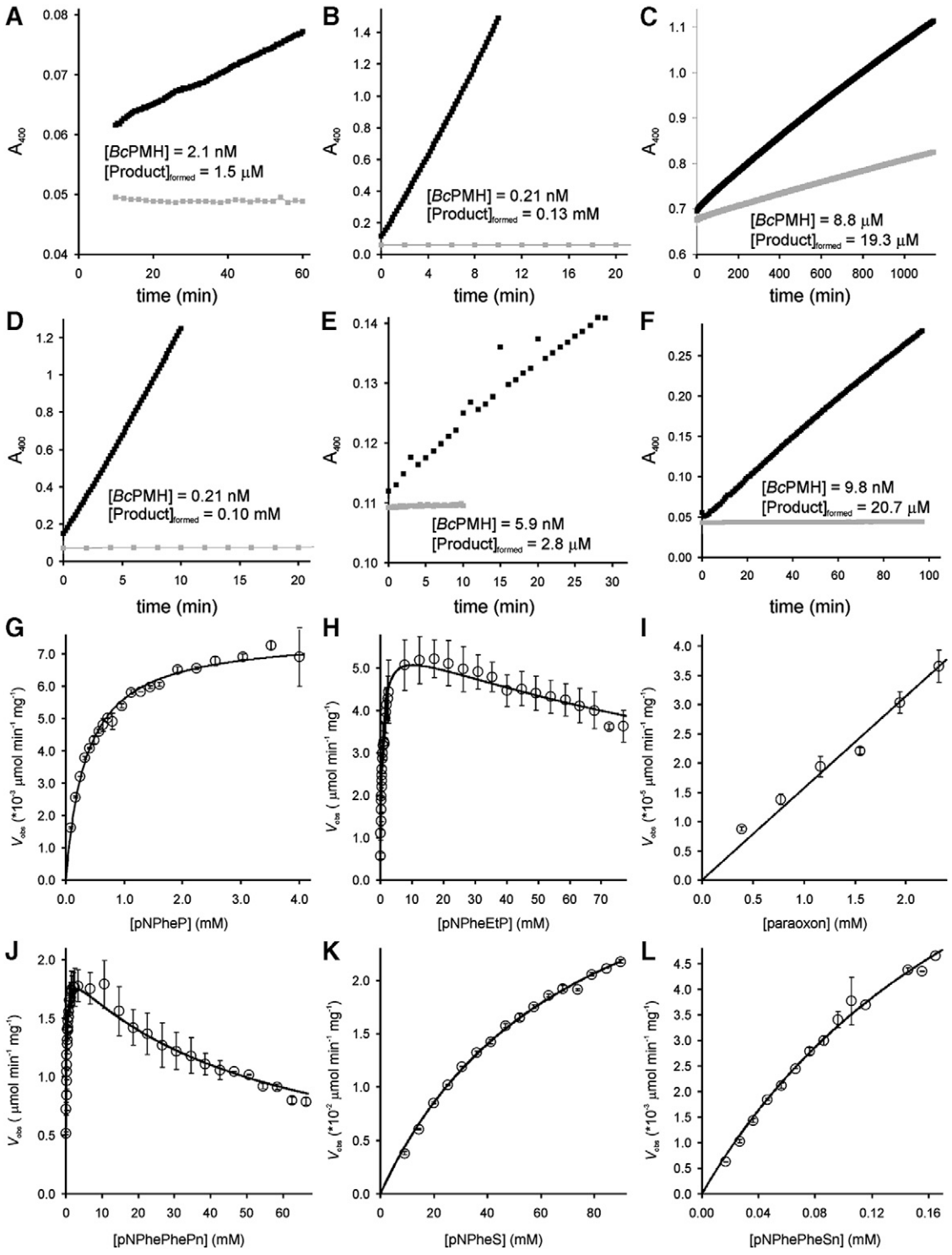

Fig. S1. Time-dependent production of *p*-nitrophenol, monitored by an increase in absorbance at 400 nm, as a result of hydrolysis of substrate **1b**–**6b** (*A*–*F*) and Michaelis–Menten curves for all reactions catalyzed by *Bc*PMH at pH 7.5 (*G*–*L*). Time courses for phosphate monoester **1b** (*A*), phosphate diester **2b** (*B*), phosphate triester **3b** (*C*), phosphonate monoester **4b** (*D*), sulfate monoester **5b** (*E*), and sulfonate monoester **6b** (*F*) in the presence (black dots) and absence (gray dots) of *Bc*PMH WT show that the number of turnovers per enzyme active site varied from at least 2 for phosphate triester **3b** to well over 10^4 for phosphate diester **2b** and phosphonate monoester **4b**. (*G*–*L*) show substrate concentration-dependent hydrolytic activity for phosphate monoester **1b** (*G*), phosphate diester **2b** (*H*), phosphate triester **3b** (*I*), phosphonate monoester **4b** (*J*), sulfate monoester **5b** (*K*), and sulfonate monoester **6b** (*L*). The curves for phosphate diester **2b** and phosphonate monoester **4b** could be fitted to a kinetic model considering substrate inhibition with K_{si} values of 169 ± 20 and 53 ± 3 mM, respectively. No saturation kinetics was observed for the enzyme-catalyzed hydrolysis of phosphate triester **3b**. Therefore the data were fitted to pseudo-first-order kinetics in which the slope directly correlates to k_{cat}/K_M.

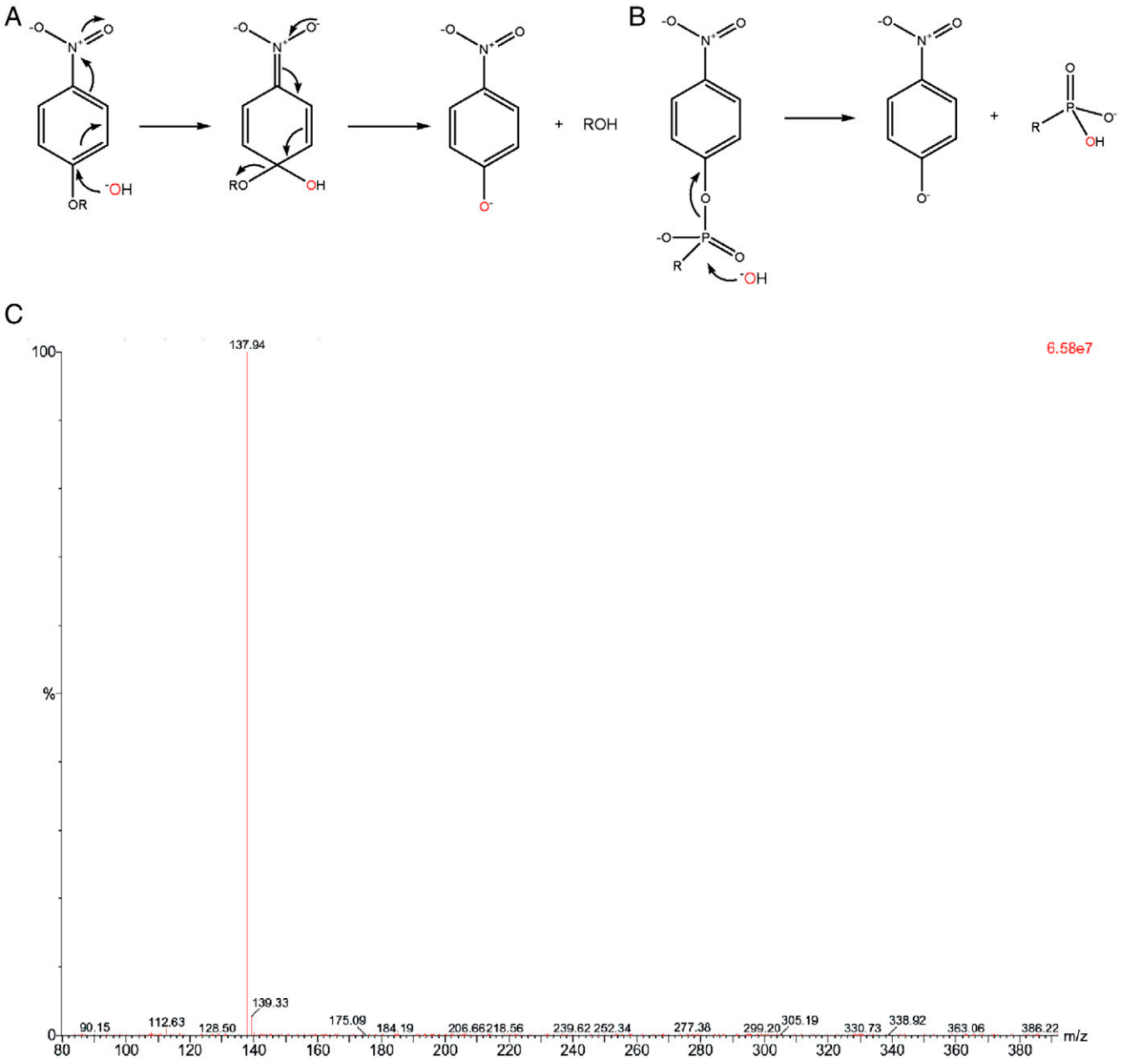

Fig. S2. Possible mechanisms for nucleophilic hydrolysis of compounds **1b**–**6b** and mass spectrometric analysis of isotope-labeled product. (*A*) Nucleophilic attack on the phenolic CO bond via a tetrahedral intermediate (S_NAr mechanism). (*B*) Nucleophilic attack on the phosphorus or sulfur center (phosphonate monoester hydrolysis shown here as an example). The oxygen atom that originates from the nucleophile (which is H_2O in the net reaction) is indicated in red. (*C*) Typical ESI-MS (ES^- signal) spectrum of *p*-nitrophenol product after the incubation of substrates **1b**–**6b** in the presence of enzyme and 9.5% ^{18}O-labeled water. The major peak at $m/z = 137.94$ corresponds to *p*-nitrophenol with no ^{18}O incorporation, that is, the result of attack of $H_2{}^{18}O$ at the phosphorus/sulfur center (*B*). No extra peak for ^{18}O-*p*-nitrophenol was observed at the expected $m/z = 139.94$ Da that would be the result of a $H_2{}^{18}O$ attack at the phenol ring by addition-elimination (*A*). The latter mechanism is thereby ruled out.

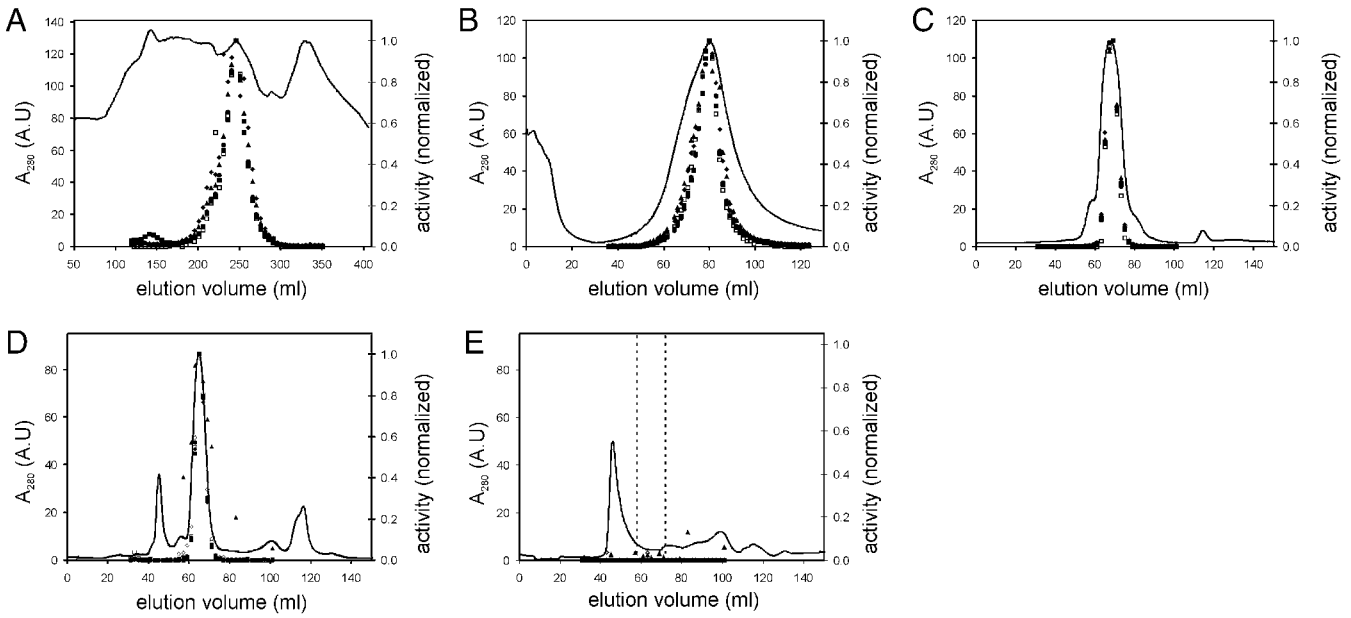

Fig. S3. Copurification of activities towards substrates **1b** (■), **2b** (♦), **3b** (▲), **4b** (●), **5b** (□), and **6b** (◇), shown together with the absorption trace at 280 nm (solid line). (*A*) anion exchange (Q-Sepharose); (*B*) hydrophobic interaction (phenyl Sepharose); (*C*) size exclusion (Superdex 200). (*D*) Size exclusion with the Strep-tagged enzyme. (*E*) Size exclusion trace of the empty plasmid purification for the strep-tactin purification procedure. The dashed vertical lines indicate the fractions that would be pooled and concentrated during the actual purification of *Bc*PMH.

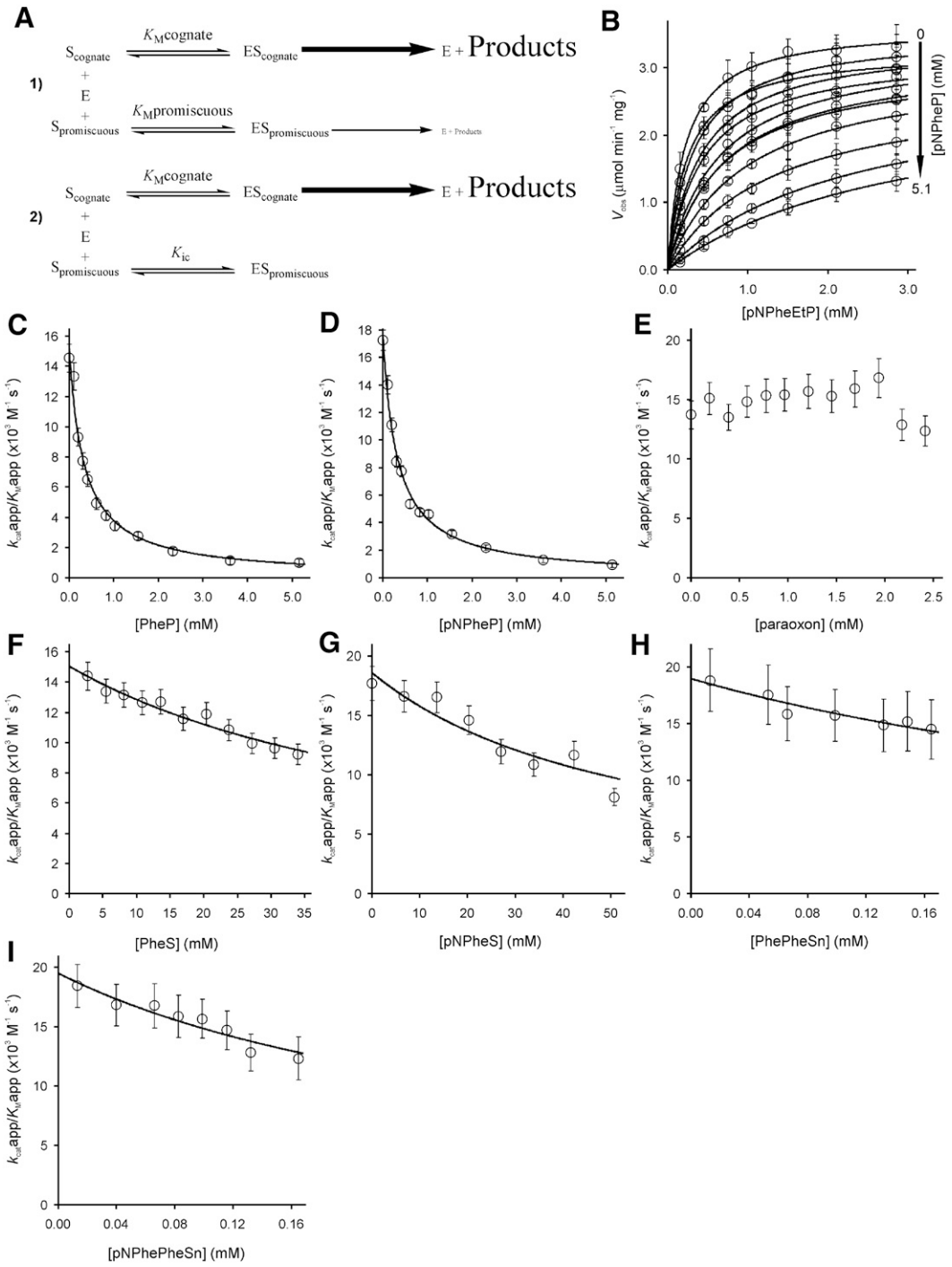

Fig. S4. Inhibition of the *Bc*PMH-catalyzed hydrolysis of phosphate diester **2b** by promiscuous substrates. (*A*) The hydrolysis rate of the cognate substrate ($S_{cognate}$) is around a 100-fold higher than that of any of the promiscuous substrates; scheme 1 can be simplified to scheme 2, in which K_{ic} should be similar to K_M promiscuous. (*B*) Michaelis–Menten plots for the hydrolysis of phosphate diester **2b** in the presence of increasing concentrations of phosphate monoester **1b** (0-0.10-0.21-0.31-0.41-0.62-0.82-1.03-1.54-2.32-3.61-5.15 mM). Each curve was fitted to $V_{obs} = V_{max}{}^{app} \times [P_{diester}\ \mathbf{2b}]/(K_M{}^{app} + [P_{diester}\ \mathbf{2b}])$. The resulting values for $V_{max}{}^{app}$ and $K_M{}^{app}$ were used to calculate $k_{cat}{}^{app}/K_M{}^{app}$. For all substrates but phosphate triester **3b**, which did not show significant inhibition, the relationship between $k_{cat}{}^{app}/K_M{}^{app}$ and the concentration of promiscuous substrate could be fitted to $k_{cat}{}^{app}/K_M{}^{app} = (k_{cat}/K_M)/(1 + [P_{monoester}\ \mathbf{1b}]/K_{ic})$. Inhibition of hydrolysis of **2b** by (*C*) phosphate monoester **1a**, (*D*) phosphate monoester **1b**, (*E*) phosphate triester **3b**, (*F*) sulfate monoester **5a**, (*G*) sulfate monoester **5b**, (*H*) sulfonate monoester **6a**, and (*I*) sulfonate monoester **6b**. The K_{ic} values for phosphate monoester **1b**, sulfate monoester **5b**, and sulfonate monoester **6b** are listed in Table 2 and are equal to their K_M values, showing that the same active site is responsible for the conversion of native and promiscuous substrates. The K_{ic}s for phosphate monoester **1b**, sulfate monoester **5b**, and sulfonate monoester **6b** are therefore equal to their K_M values for conversion and are listed in Table 1. The k_{cat} values for these compounds were determined by fitting a time course of their hydrolysis to Eqs. S3 and S4.

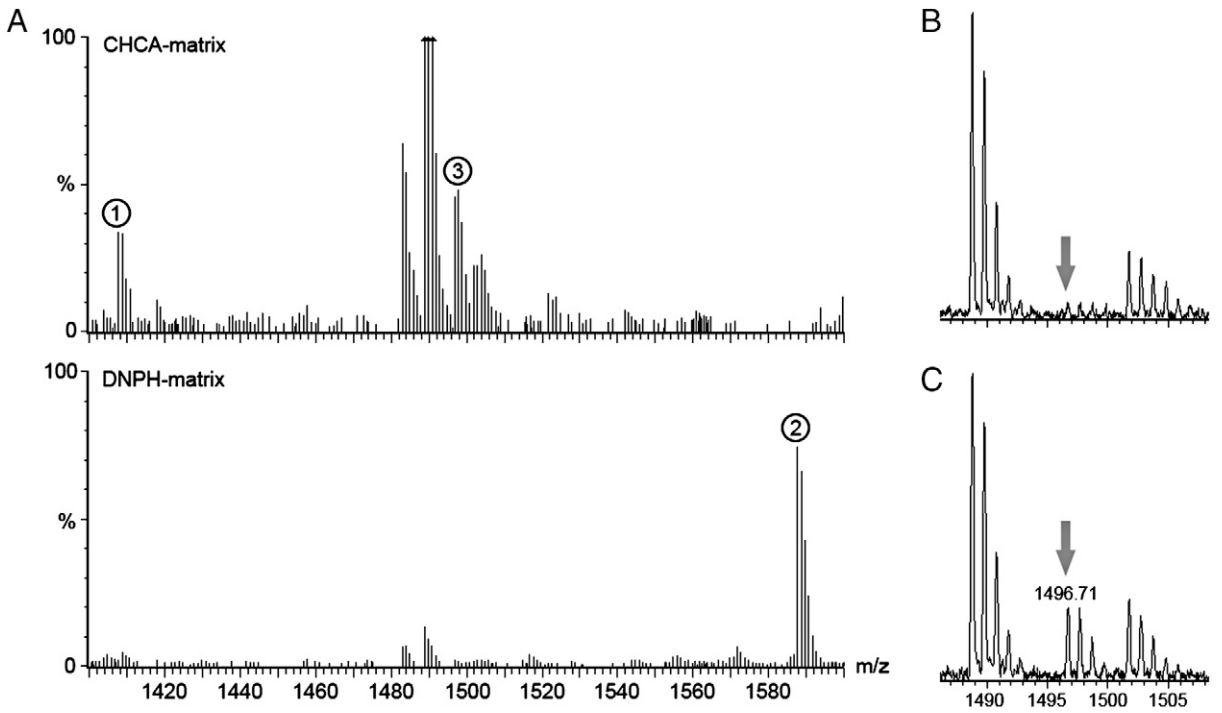

Fig. S5. Mass spectrometric analysis of *Bc*PMH to prove the presence of fGly at residue 57 under aerobic expression and increased Cys57 content after anaerobic expression. (*A*) MALDI-TOF mass spectrometric analysis of Strep-*Bc*PMH indicates the presence of a fGly at residue 57. Comparison of the mass spectra from a tryptic digest of *Bc*PMH, which was alkylated with acrylamide, in an α-cyano-4-hydroxycinnamic acid (CHCA) matrix and a matrix supplemented with 2,4-dintrophenylhydrazine (DNPH). Signal 1, corresponding to the peptide containing residue 57 (molecular mass = 1407.7 Da), is shifted 180 Da upon treatment with DNPH (peak 2), which indicates the presence of a fGly. However, the alkylated peptide containing unmodified Cys (molecular mass = 1496.7 Da) is also detected (peak 3). (*B*, *C*) MALDI-TOF analysis of tryptic digests of *Bc*PMH coexpressed with *Mtb*FGE (*B*) and anaerobically expressed *Bc*PMH (*C*) in a CHCA matrix. Under anaerobic conditions the peptide 49-NHVTTCVPCGPAR-61 containing Cys57 is detected (alkylated with two equivalents of acrylamide, *M* = 1496.71 Da), whereas it is not detectable above background in the protein coexpressed with *Mtb*FGE. This indicates that fGly modification is compromised under anaerobic conditions as described before (18) and the fraction of Cys57 vs. fGly57 is increased in this protein preparation. The fGly57-containing peptide did not yield signals above background for both enzyme preparations.

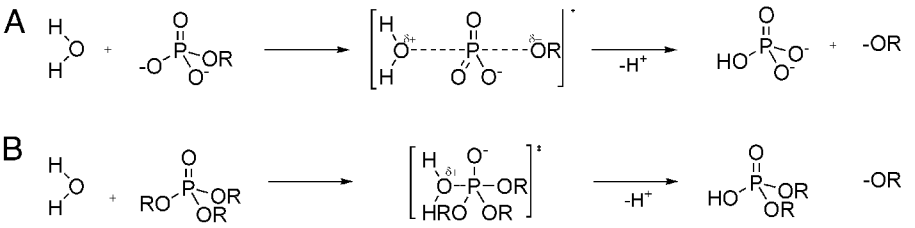

Fig. S6. The differing nature of the transition states for uncatalyzed hydrolysis of the substrates used in this study. (*A*) Dissociative transition states are characterized by a high degree of bond breaking and little bond making. Large negative Brønsted values (β_{lg}) suggest that charge accumulation is located primarily at the leaving group ($^{-}$OR). The dianionic form of a phosphate monoester (**1a,b**) is shown here as an example. In addition the monoanionic form of sulfate monoester (**5a,b**) is hydrolyzed via this mechanism in solution (19–21). (*B*) Associative transition states are characterized by a larger degree of bond making between the incoming nucleophile and the reaction center. In comparison to the dissociative mechanism, more charge accumulates at the phosphoryl oxygens and less at the leaving group (resulting in a less negative β_{lg}). Phosphate diesters **2a,b** (22), phosphate triester **3b** (23), phosphonate monoesters **4a,b** (24), and sulfonate monoesters **6a,b** (25) are hydrolyzed via this associative pathway.

Table S1. Rate constants for the uncatalyzed hydrolysis of substrates 1–6 at pH 7.5; 30 °C

Substrate	k_{uncat}* (s^{-1})	k_w* ($M^{-1}\,s^{-1}$)
1a†	1.2×10^{-10}	2.2×10^{-12}
1b‡	4.3×10^{-9}	7.8×10^{-11}
2a§	4.0×10^{-14}	7.3×10^{-16}
2b¶	2.6×10^{-13}	4.7×10^{-15}
3b	5.1×10^{-8}	9.2×10^{-10}
4a	1.8×10^{-13}	3.3×10^{-15}
4b	1.7×10^{-11}	3.1×10^{-13}
5a‖	4.3×10^{-13}	7.8×10^{-15}
5b**	1.1×10^{-9}	2.0×10^{-11}
6a	1.4×10^{-10}	2.6×10^{-12}
6b	5.5×10^{-9}	1.0×10^{-10}

*Based on either published k_{uncat} or k_w. k_{uncat} and k_w are correlated via the formula $k_{uncat} = k_w \times [H_2O]$, in which $[H_2O]$ in a normal aqueous solution is 55 M.

†Derived from the rate constants for the mono- and dianionic states of **1a**, assuming the pK_a of the equilibrium between the mono- and dianion of **1a** to be 5. The $k_{monoanion}$ was calculated from the published $\Delta H^{\ddagger}$ and $\Delta S^{\ddagger}$ values (26). The $k_{dianion}$ was calculated from the published Brønsted relation for the hydrolysis of phosphate monoester dianions ($\beta_{lg} = 1.23$; ref. 26) and the $k_{dianion}$ of phosphate monoester **1b**, assuming pK_a values of 7.14 and 9.98 for *p*-nitrophenol and phenol, respectively. The $k_{dianion}$ for **1b** was calculated from the published $\Delta H^{\ddagger}$ and $\Delta S^{\ddagger}$ values (27).

‡Derived from the rate constants for the mono- and dianionic states of **1b**, assuming the pK_a of the equilibrium between the mono- and dianion of **1b** to be 5. The values for $k_{monoanion}$ and $k_{dianion}$ were calculated from the published $\Delta H^{\ddagger}$ and $\Delta S^{\ddagger}$ values for both species (26, 27).

§Derived from Chin et al. (28), by using the published Brønsted relationship and temperature dependence.

¶Derived from Purcell and Hengge (29), by using the published temperature dependence for k_{OH} and extrapolation to k_{uncat} at pH 7.5 ($[^{-}OH] = 10^{-(14-7.5)} = 3.2 \times 10^{-7}$ M).

‖Derived from k_{uncat} for sulfate monoester **5b** by using the published Brønsted relation (30) ($\beta_{lg} = -1.20$, pK_a for *p*-nitrophenol is 7.14, and pK_a for phenol is 9.98).

**Nikolic-Hughes et al. (31), assuming that sulfate monoester hydrolysis is mostly pH-independent in between pH 4 and 12 (32).

Table S2. Comparison of the kinetic parameters of *Bc*PMH wild type and Cys-only for *p*-nitrophenol substrates 1b–6b at pH 7.5

Substrate	Wild-type			Cys-only mutant			Ratio (wild type: Cys-only mutant)		
	k_{cat} (s^{-1})	K_M (mM)	k_{cat}/K_M ($M^{-1}\,s^{-1}$)	k_{cat} (s^{-1})	K_M (mM)	k_{cat}/K_M ($M^{-1}\,s^{-1}$)	k_{cat}	K_M	k_{cat}/K_M
1b	$(7.7 \pm 0.1) * 10^{-3}$	0.35 ± 0.02	22 ± 1	$(1.4 \pm 0.2) * 10^{-3}$	0.27 ± 0.02	5.2 ± 0.8	5.5	1.3	4.2
2b	5.8 ± 0.1	0.63 ± 0.04	$(9.2 \pm 0.6) * 10^{3}$	1.4 ± 0.3	1.6 ± 0.4	$(8.8 \pm 2.9) * 10^{2}$	4.1	0.39	10
3b	$>3.7 * 10^{-5}$	>2.4	$(1.6 \pm 0.1) * 10^{-2}$	$>6.6 * 10^{-5}$	>2.4	$(2.9 \pm 0.1) * 10^{-2}$	-	-	0.56
4b	2.73 ± 0.06	0.19 ± 0.02	$(1.5 \pm 0.1) * 10^{4}$	0.34 ± 0.01	0.14 ± 0.01	$(2.4 \pm 0.2) * 10^{3}$	8.0	1.4	6.3
5b	$(4.0 \pm 0.1) * 10^{-2}$	68 ± 4	0.59 ± 0.04	ND	ND	ND	-	-	-
6b	$(1.2 \pm 0.1) * 10^{-2}$	0.24 ± 0.03	49 ± 7	-	-	0.82 ± 0.04	-	-	60

Table S3. Statistics for data collection and structure refinement of Strep*Bc*PMH

Data collection	
Space group	$P2_12_12_1$ (19)
Unit cell dimensions	$a = 57.7$, $b = 200.1$, $c = 211.7$, $\alpha = \beta = \gamma = 90°$
Beam line	Rotating copper anode (Rigaku Ru-H3R)
l (Å)	1.5418
Resolution limit (Å)	2.4
R_{merge} [highest resolution shell]	0.14 [0.61]
Number of reflections	504,035 [46,820]
Number of unique reflections	96,059 [10,566]
Completeness %	98.9 [95.9]
$I/I\sigma$	11.5 [2.5]
Refinement	
R	0.182
R_{free}	0.239
rmsd bonds	0.015
rmsd angles	1.554
Residues in the most allowed regions of Rachamandran plot %	97.4